

1 A single-column ocean-biogeochemistry model (GOTM-TOPAZ) 2 version 1.0

3 Hyun-Chae Jung¹, Byung-Kwon Moon¹, Jieun Wie¹, Hye-Sun Park², Johan Lee³, Young-Hwa Byun³

4 ¹Division of Science Education, Institute of Fusion Science, Chonbuk National University, Jeonju 54896, South Korea

5 ²Cray Korea Inc., Seoul 08511, South Korea

6 ³National Institute of Meteorological Sciences, Seogwipo 63568, South Korea

7 *Correspondence to:* Byung-Kwon Moon (moonbk@jbnu.ac.kr)

8 **Abstract.** Recently, Earth System Models (ESMs) have begun to consider the marine ecosystem to reduce errors in climate
9 simulations. However, many models are unable to fully represent the ocean biology-induced climate feedback, which is due
10 in part to significant bias in the simulated biogeochemical properties. Therefore, we developed the Generic Ocean
11 Turbulence Model–Tracers of Phytoplankton with Allometric Zooplankton (GOTM-TOPAZ), a single-column ocean
12 biogeochemistry model that can be used to improve ocean biogeochemical processes in ESMs. This model was developed by
13 combining the GOTM, a single-column model that can simulate the physical environment of the ocean, and TOPAZ, a
14 biogeochemical module. Here, the original form of TOPAZ has been modified and modularized to allow easy coupling with
15 other physical ocean models. To demonstrate interactions between ocean physics and biogeochemical processes, the model
16 was designed to allow ocean temperature to change due to absorption of visible light by chlorophyll in phytoplankton. We
17 also added a module to reproduce upwelling and the air-sea gas transfer process for oxygen and carbon dioxide, which are of
18 particular importance for marine ecosystems. The GOTM-TOPAZ simulated variables (e.g., chlorophyll, oxygen, nitrogen,
19 phosphorus, silicon) were evaluated by comparing against observations. **The temporal variability of observed upper-ocean
20 (0-20m) chlorophyll is well captured by GOTM-TOPAZ model with a correlation coefficient of 0.51. The surface correlation
21 coefficients between the GOTM-TOPAZ oxygen, nitrogen, phosphorus, and silicon are 0.47, 0.30, 0.16, and 0.19,
22 respectively. We also compared the GOTM-TOPAZ simulations with those from the MOM-TOPAZ and found that GOTM-
23 TOPAZ showed relatively lower correlations, which is most likely due to a limitation of single-column model. Despite this
24 limitation, we argue that our GOTM-TOPAZ is a good starting point for further investigation of key biogeochemical
25 processes and also is useful to couple complex biogeochemical processes with various oceanic global circulation models.**

26

27 1 Introduction

28 Over several decades, climate researchers have accumulated significant knowledge on atmosphere-land-ocean feedback
29 processes through various studies related to climate systems (Friedlingstein et al., 2006; Soden and Held, 2006; Dirmeyer et
30 al., 2012; Randerson et al., 2015). With the advancement of coupled modeling techniques and an exponential increase in the

31 number of computer resources available, climate research institutions worldwide began competing to develop earth system
32 models (ESMs) (Dunne et al., 2012a; Dunne et al., 2012b; Jones and Sellar, 2015; Sokolov et al., 2018). ESMs are often
33 coupled with biogeochemistry models that consider the atmosphere–ocean carbon cycle and ocean ecosystem cycles (Dunne
34 et al. 2012b; Yool et al., 2013; Azhar et al., 2014; Stock et al., 2014; Aumont et al., 2015). Recently, reproductions of ocean
35 ecosystems in ESMs has become very precise with the addition of physiological details, such as light or nutrient acclimation,
36 and the division of various phytoplankton and zooplankton into functional groups (Hense et al., 2017).

37 The following processes are generally considered the most important in ocean biogeochemistry models: the ocean
38 ecosystem cycle, including phytoplankton and zooplankton; the biogeochemical carbon cycle; and the biogeochemical cycle
39 of key nutrients (P, N, Fe, and Si) (Dunne et al., 2012b; Aumont et al., 2015). These three cycles are not independent and
40 include mutual material exchange through chemical mechanisms. **There are still no accurate methodologies with which to**
41 **distinguish biogeochemical variables and to represent biogeochemical processes as formulas (Sauerland et al., 2018).** In
42 other words, biogeochemical processes are reproduced in the model via parameterization that adjusts the parameters of a
43 formula based on observations and some general parameters (e.g., maximum phytoplankton growth rate) that are adjusted
44 until the model produces reasonable results (Sauerland et al., 2018).

45 Researchers have been using single-column models (SCMs) to control the parameterization and increase their
46 understanding of the physical processes in models. Betts and Miller (1986) suggested that SCMs were an effective tool with
47 which to develop and control the convective scheme of an atmospheric model, while Price et al. (1986) used an ocean SCM
48 to study the daily cycle of the mixed layer in the Pacific Ocean. An SCM allows the control of physics parameters, alongside
49 large-scale forcing influences, and unlike 3D models it has a low calculation cost. Accordingly, SCMs have been viewed as
50 essential tools with which to develop and improve numerical models (Lebassi-Habtezion and Caldwell, 2015; Hartung et al.,
51 2018). SCM-based studies are essential for improving ocean-biogeochemical processes which reproduced in climate models
52 based on column physics (Evans and Garçon, 1997; Burchard et al., 2006; Bruggenman and Bolding, 2014). Even the latest
53 analyses of the ESMs included in the Coupled Model Intercomparison Project Phase 5 (CMIP5) show high biases and inter-
54 model diversity in ocean biogeochemical variables (Lim et al., 2017). Therefore, a single-column form of a biogeochemistry
55 model might be a useful tool to meet the ongoing demand for improvements in the biogeochemistry models the ESMs.

56 The oceanic biogeochemical cycle affects not only the physical environment of the upper ocean but also that of the entire
57 climate system, and such changes produce feedback that, in turn, alters the ocean ecosystem (Hense et al., 2017; Lim et al.,
58 2017; Park et al., 2018). Hense et al. (2017) presented the CO₂ cycle, gas and particle cycle, and changes in the physical
59 environment of the upper ocean by chlorophyll as important climate-ocean biogeochemistry feedback loops reproduced in
60 ESMs that are currently available. An ESM that reproduces all three of these biological mechanisms does not exist today;
61 however, all of these mechanisms need to be properly reproduced in the ESMs to reduce the uncertainty in predicting future
62 climate change. This would allow ESMs to change in a fundamentally different way. Furthermore, there are generally time
63 constraints in repeated experiments using ocean general circulation models (OGCMs) and biogeochemistry models due to

64 their complexity and the heavy calculation required. Consequently, SCMs are crucial for applying and testing new climate-
 65 ocean-biogeochemistry feedbacks in existing ESMs.

66 In this study, we developed the Generic Ocean Turbulence Model–Tracers of Phytoplankton with Allometric Zooplankton
 67 (GOTM-TOPAZ), which is a single-column ocean-biogeochemistry model. GOTM is a one-dimensional ocean model that
 68 focuses on reproducing statistical turbulence closures (see <http://www.gotm.net>); TOPAZ is an ocean-biogeochemistry
 69 model developed by the Geophysical Fluid Dynamics Laboratory (GFDL) and coupled with the ESM2M and ESM2G
 70 models (Dunne et al., 2012a; Dunne et al., 2012b). We modularized TOPAZ to apply external physical environmental data
 71 while modifying it as an SCM. It was then combined with a GOTM utilizing an air-sea gas exchange for CO₂ and O₂ and
 72 optical feedback from photosynthesis by chlorophyll. A w-advection prescription module that can reproduce upwelling was
 73 also added to this model. To verify GOTM-TOPAZ, we selected points in the East/Japan Sea off the coast of the Korean
 74 Peninsula upon which to conduct simulations. The results produced by the model were compared to observed data and
 75 results from OGCMs to verify its reliability.

76

77 **2 The Physical Ocean Model: General Ocean Turbulence Model (GOTM)**

78 In GOTM-TOPAZ, the GOTM version 4.0 is applied to ocean physics. The physical bases of the GOTM are Reynolds-
 79 averaged Navier–Stokes equations in a rotational coordinate system (Eqs. 1 and 2). Moreover, the temperature and salinity
 80 equations derived using these methods are given in Eqs. 3 and 4, respectively. GOTM uses one-dimensional potential
 81 temperature, salinity, and horizontal velocity based on these four equations, as shown below:

82

$$83 \quad \partial_t u - \nu \partial_{zz} u + \partial_z \langle u'w' \rangle = -\frac{1}{\rho_0} \partial_x p + f v \quad (1)$$

$$84 \quad \partial_t v - \nu \partial_{zz} v + \partial_z \langle v'w' \rangle = -\frac{1}{\rho_0} \partial_y p - f u \quad (2)$$

$$85 \quad \partial_t T - \nu' \partial_{zz} T + \partial_z \langle w'T' \rangle = \frac{\partial_z I}{c_p \rho_0} \quad (3)$$

$$86 \quad \partial_t S - \nu'' \partial_{zz} S + \partial_z \langle w'S' \rangle = \tau_R^{-1} (S_R - S). \quad (4)$$

87

88 In Eqs. (1) and (2), u , v and w represent the mean velocities in the spatial directions x (eastward), y (northward), and z
 89 (upward), respectively; ν represents the molecular diffusivity of momentum; ρ_0 represents a constant reference density; p
 90 represents pressure; and f represents the Coriolis parameter. In Eq. (3), the temperature (T) equation, ν' represents the
 91 molecular diffusivity due to heat; c_p represents the heat capacity; and I represents the vertical divergence of short-wave
 92 radiation. The effect of solar radiation absorbed by seawater is included in this equation; thus, Eq. (3) is closely associated
 93 with the radiation parameterization method. Moreover, a coupled ocean biogeochemistry model must contain an additional

94 short-wave absorption process associated with chlorophyll synthesis distributed throughout the upper-ocean layer (Morel and
95 Antoine, 1994; Cloern et al., 1995; Manizza et al., 2005; Litchman et al., 2015; Hense et al., 2017). Based on the
96 methodology of Manizza et al. (2005), we applied a visible light absorption process due to chlorophyll synthesis, explained
97 in detail in Sect 4.4, to the coupled model. Equation (4) explains the vertical distribution of salinity (S). In this equation, v''
98 represents the molecular diffusivity of salinity; τ_R represents the relaxation time scale; and S_R represents the observed
99 salinity distribution. In other words, the terms on the right side of this equation express the “relaxation” process based on
100 observations. Unlike 3D models, SCMs cannot reproduce horizontal advection. Therefore, as salinity is greatly affected by
101 horizontal advection, it is necessary to prescribe and supplement the observed value to the simulated value with the terms on
102 the right side of Eq. (4) (Burchard et al., 2006). Please see Umlauf and Burchard (2003, 2005), Umlauf et al. (2005), , and
103 Burchard et al. (2006) for further detailed information on the GOTM.

104

105 **3 The Ocean Biogeochemistry Model: Tracers of Phytoplankton with Allometric Zooplankton (TOPAZ)**

106 We chose TOPAZ version 2.0 version to couple with the GOTM. TOPAZ simulates the nitrogen, phosphorus, iron,
107 dissolved oxygen, and lithogenic material cycles as well as the ocean carbon cycle while also considering zooplankton and
108 phytoplankton growth cycles. It divides phytoplankton into small and large groups based on size, and the group of nitrogen-
109 fixing diazotrophs. Consequently, TOPAZ handles a total of 30 prognostic and 11 diagnostic tracers. The local changes in
110 the tracers simulated in TOPAZ can be explained by the following equation:

111

$$112 \partial_t C = -\nabla \cdot \vec{v}C + \nabla K \nabla C + S_C \quad (5)$$

113

114 Equation (5) is an advection-diffusion equation for each state variable C simulated in TOPAZ. In this equation, \vec{v}
115 represents the velocity vector calculated in the ocean model, K represents diffusivity, and S_C represents the sources minus the
116 sinks of C calculated at each point in the model. TOPAZ receives input from the ocean model in terms of the transport
117 tendency of the tracers associated with advection and horizontal diffusion; for vertical diffusion, it calculates the value of the
118 sources minus the sinks internally. The biological processes of TOPAZ were reproduced with a focus on phytoplankton
119 growth, nutrient and light limitations, the grazing process, and empirical formulas derived from observations. These are
120 followed by the Redfield ratio (Redfield et al., 1963), Liebig’s law of the minimum (de Baar, 1994), and size considerations
121 (large organisms feed on smaller ones), which were used to establish the ocean ecosystem model (Dunne et al., 2012b).
122 Please see Dunne et al. (2012b) for further detailed information on TOPAZ.

123

124 **4 The Ocean Biogeochemistry Coupled Model: GOTM-TOPAZ**

125 TOPAZ was initially coupled with Modular Ocean Model 5 (MOM5), an OGCM developed by the GFDL. We separated
126 TOPAZ from MOM5 and constructed two modules by separating the initialization and main calculation subroutines. This
127 model was then modified into an SCM while adding interfaces associated with surface flux prescriptions (boundary
128 conditions) and initial data input.

129 In our new coupled model, the GOTM provided ocean physics calculations for TOPAZ and TOPAZ relayed optical
130 feedback from the chlorophyll simulated according to these data to GOTM. A subroutine that calculates the optical feedback
131 from chlorophyll and another that prescribes the w-advection were added to GOTM-TOPAZ (see Fig. 1 for the flow
132 diagram). Upwelling that usually occurs along coastal areas due to wind plays a major role in changing the vertical
133 distribution of zooplankton and phytoplankton by supplying the surface layer with nutrient-rich intermediate water (Krezel et
134 al., 2005; Lips and Lips, 2010; Shin et al., 2017). **We connected the w-advection module in GOTM to TOPAZ so that the
135 upwelling was reproduced in TOPAZ.**

136

137 **4.1 Initial Conditions**

138 The initial data needed to run GOTM-TOPAZ can be divided into the data needed to operate the GOTM and TOPAZ models
139 individually. **To run the GOTM, it is necessary to have the ocean (temperature and salinity) initial data and the salinity data
140 for the duration of the model run time.** The latter are needed to relax the GOTM. For TOPAZ, initial data are needed for the
141 30 prognostic and 11 diagnostic tracers.

142

143 **4.2 Boundary Conditions**

144 Atmospheric forcing data must be prescribed in GOTM-TOPAZ because it is not coupled with an atmospheric model. The
145 atmospheric forcing variables needed to run the model are: 10 m u-wind; v-wind [m s^{-1}]; surface (2 m) air pressure [hPa];
146 surface (2 m) air temperature [$^{\circ}\text{C}$]; relative humidity [%], wet bulb temperature [$^{\circ}\text{C}$], or dew point temperature [$^{\circ}\text{C}$]; and
147 cloud cover [1/10].

148 Values for surface or bottom fluxes for a few types of tracers must be provided to accurately simulate ocean
149 biogeochemical variables. **TOPAZ includes processes for variables include sediment calcite cycling and the external bottom
150 fluxes of O_2 , NH_4 , PO_4 , and alkalinity (Dunne et al., 2012b).** However, it does not include a process for calculating
151 atmosphere-ocean surface flux. Therefore, we added processes for calculating the surface fluxes of O_2 , NO_3 , NH_4 , alkalinity,
152 lithogenic aluminosilicate, dissolved iron, and dissolved inorganic carbon. Of the subroutines shown in Fig. 1., the
153 calculation of the surface fluxes is implemented using generic_topaz_column_physics. The surface flux of NO_3 , NH_4 ,
154 lithogenic aluminosilicate, and dissolved iron is prescribed using monthly average climate values, while alkalinity is

155 calculated from prescribed NO_3 dry/wet deposition values. These surface flux data are provided by the Australian Research
 156 Council's Centre of Excellence for Climate System Science (ARCCSS; <http://climate-cms.unsw.wikispaces.net/Data>). The
 157 following equation was used to calculate the air-sea gas transfer for O_2 and CO_2 (dissolved inorganic carbon):

158

$$159 \quad F = k_w \rho ([A] - [A]_{\text{sat}}) \quad (6)$$

160

161 Here, F is the upward flux of gas A and k_w is its gas transfer velocity, which can be calculated as a function of the
 162 Schmidt number and wind speed at 10 m (Wanninkhof, 1992). ρ is the density of surface seawater, $[A]$ is the concentration
 163 [$\mu\text{mol kg}^{-1}$] of gas A at the surface of the ocean, and $[A]_{\text{sat}}$ is the corresponding saturation concentration of gas A in
 164 equilibrium with a water vapor-saturated atmosphere at total atmospheric pressure (Najjar and Orr, 1998). $[A]$ is predicted by
 165 the model. Please see Najjar and Orr (1998) for further detailed information related to Eq. (6).

166

167 4.3 Ocean Physics

168 The GOTM simulates the physics of oceanic environments based on Eqs. (1)–(4). In the coupled model, the GOTM relays
 169 the following simulated one-dimensional ocean physical variables to the TOPAZ module at each time step: potential
 170 temperature [$^{\circ}\text{C}$]; salinity [psu]; thermal diffusion coefficient [$\text{m}^2 \text{sec}^{-1}$]; density [kg m^{-3}]; thickness [m]; mixed layer
 171 thickness [m]; and radiation [w m^{-2}].

172

173 4.4 Optical Feedback

174 As explained in Sect. 2, the photosynthesis of chlorophyll distributed throughout the upper ocean is known to have physical
 175 effects. Manizza et al. (2005) used satellite observation data and OGCMs to conduct a study of changes in ocean irradiance
 176 due to the absorption of visible light by chlorophyll. We used their methodology to apply the optical feedback from
 177 chlorophyll on GOTM-TOPAZ in the following manner:

178

$$179 \quad k_{\lambda} = k_{\text{sw}(\lambda)} + \chi_{(\lambda)} \cdot [\text{chl}]^{e_{(\lambda)}} \quad (7)$$

$$180 \quad I_{\text{IR}} = I_0 \cdot 0.58 \quad (8)$$

$$181 \quad I_{\text{VIS}} = I_0 \cdot 0.42 \quad (9)$$

$$182 \quad I_{\text{RED}} = I_{\text{BLUE}} = \frac{I_{\text{VIS}}}{2} \quad (10)$$

$$183 \quad I_{(z)} = I_{\text{IR}} \cdot e^{-k_{\text{IR}z}} + I_{\text{RED}(z-1)} \cdot e^{-k_{(r)}\Delta z} + I_{\text{BLUE}(z-1)} \cdot e^{-k_{(b)}\Delta z} \quad (11)$$

184

185 In these equations, visible light was divided into red and blue/green bands in accordance with Manizza et al. (2005). In Eq.
186 (7), λ represents the wavelength of these bands and $k_{sw(\lambda)}$ represents the light attenuation coefficient of optically pure
187 seawater, which has values of 0.225 m^{-1} and 0.0232 m^{-1} , respectively, in red and blue/green bands. In these bands, the
188 values of the pigment adsorption $\chi_{(\lambda)}$ are 0.037 and $0.074 \text{ m}^{-2} \text{ mg Chl m}^{-3}$, respectively; $e_{(\lambda)}$, the power law for absorption,
189 has values of 0.629 and 0.674 [no units], respectively. Moreover, [chl] represents the concentration of chlorophyll in
190 mg Chl m^{-3} .

191 Infrared light (I_{IR}) and visible light (I_{VIS}) that reach mean open ocean conditions are set in Eqs. (8) and (9), respectively,
192 by default. However, GOTM-TOPAZ can change the light extinction method by modifying the namelist in the GOTM (see
193 <http://www.gotm.net>) and this can also be used to change the coefficients of I_{IR} and I_{VIS} . The total irradiance of the red and
194 blue/green bands that reach the ocean surface is represented in Eq. (10). Ultimately, the irradiance of visible light transmitted
195 at each vertical level (z) can be calculated in GOTM-TOPAZ using Eq. (11). Moreover, the sum of the second and third
196 terms on the right side of Eq. (11) represents photosynthetically active radiation (PAR), and is used in TOPAZ to calculate
197 the growth rate of phytoplankton groups.

198

199 **4.5 w-advection**

200 As mentioned at the beginning of Sect. 4, the upwelling phenomenon generated by coastal winds is known to affect
201 phytoplankton growth by supplying nutrient-rich intermediate water to the upper ocean. The GOTM is already designed to
202 allow users to prescribe w-advection to experiments. Therefore, we linked the subroutines of the GOTM that are related to
203 w-advection to TOPAZ, so GOTM-TOPAZ users can study the impact of upwelling on the biogeochemical environment of
204 the ocean. Users can prescribe vertical advection as a constant or input the velocities by time and depth in ASCII format to
205 reproduce the desired form of vertical motions. Please refer to the GOTM homepage (<http://www.gotm.net>) and Burchard et
206 al. (2006) for further technical details and numerical analysis of the w-advection in GOTM.

207

208 **5 Experimental setup**

209 The East/Japan Sea is unique, with its steep topography and three large, deep, and semi-enclosed basins. Moreover, it is
210 somewhat isolated from other major oceans, connects to the Pacific Ocean through a narrow strait and is sometimes referred
211 to as a miniature ocean since it contains a double gyre and experiences various oceanic phenomena (Ichiye, 1984). The high-
212 temperature, high-salinity Tsushima Warm Current (TWC) introduced through the Korea Strait is divided into two main
213 branches: the nearshore branch, which flows northeastward along the Japanese coast and the East Korea Warm Current
214 (EKWC), which flows northward along the Korean coast (Uda, 1934; Tanioka, 1968; Moriyasu, 1972) (Fig. 2). Apart from
215 these two main branches, there is another that exists offshore of the first branch, but it is not present all year (Shimomura and

216 Miyata, 1957; Kawabe, 1982). To the north, the North Korean Cold Current (NKCC) flows southward along the Korean
217 coast. Furthermore, the 200–400 m East Sea Intermediate Water (ESIW) is known for its high concentration of dissolved
218 oxygen and the appearance of a salinity-minimum layer (Kim and Chung, 1984; Kim and Kim, 1999). **The East/Japan Sea is**
219 **divided into warm and cold regions relative to the 40° N parallel, and, since the current pattern and characteristics of the**
220 **East/Japan Sea vary spatially and seasonally, this region is very important to oceanographic studies.** This region is also
221 considered important for biogeochemical research (Joo et al., 2014; Kim et al., 2016; Shin et al., 2017) for the following
222 reasons: the nutrient-rich seawater that flows along the southern coast of the Korean Peninsula due to inflow from the
223 Nakdong River, which is located at its southeastern end; the influence of a strong southerly wind during the summer, which
224 causes upwelling off the coast of the East/Japan Sea, the transport of this nutrient- and chlorophyll-rich seawater near
225 Ulleungdo Island by the EKWC. **We selected three points that have features typical of the East/Japan Sea and for which**
226 **observation data suitable to use for verification exists (Fig. 2): point 107, where the EKWC and NKCC meet (130.0° E, 38.0°**
227 **N); point 104, which is an important location along the EKWC (131.3° E, 37.1° N); and point 102, which is in the middle of**
228 **a warm eddy created as the EKWC moves north (130.6° E, 36.1° N). As noted previously, these points are in regions with**
229 **strong advection and thus may not be suitable for testing GOTM-TOPAZ, which is an SCM. However, since the results**
230 **obtained using GOTM-TOPAZ were significant when compared to the observations, we think that this shows that it is**
231 **possible to perform sensitivity experiments using GOTM-TOPAZ at several kinds of locations.**

232 The observed data such as seawater temperature and salinity was used to initialize and relax vertical structures in the
233 GOTM throughout the simulation. This data was provided by the National Institute of Fisheries Science (NIFS;
234 <http://www.nifs.go.kr/kodc>). The water temperature and salinity data from the NIFS was measured at 15 m intervals at
235 depths of 0 m to 500 m. They were measured once in February, April, June, August, October, and December every year from
236 1961 to date. For the initial data on prognostic/diagnostic tracers in TOPAZ, we used the data provided by ARCCSS for use
237 with MOM5 (<http://climate-cms.unsw.wikispaces.net/Data>). This initial tracer data was interpolated for each location, and a
238 spin-up was applied over 14 years for use in the experiments. For atmospheric forcing data, we input 0.75° ERA-Interim
239 reanalysis data provided by the European Centre for Medium Range Weather Forecasts (Dee et al., 2011). We applied global
240 data to our model by interpolating the latitude and longitude values of the test points.

241 We used the monthly average of observed seawater temperature and salinity data from the analysis fields in the EN.4.2.1,
242 provided by the Hadley Centre at the Met Office (Good et al., 2013) to verify the results from GOTM-TOPAZ following the
243 adjusted method in Gouretski and Reseghetti (2010). With respect to chlorophyll, we compared the results simulated by the
244 model using observational data with a resolution of 9 km gathered by the NASA Goddard Space Flight Center's Sea-
245 Viewing Wide Field-of-View Sensor (SeaWiFS) from October 1997 to December 2007 (McClain et al., 1998). The results of
246 simulations of dissolved oxygen and nutrients such as nitrogen, phosphorus, and silicon were tested using observational data
247 from the NIFS; **these data were measured once every year, in February, April, June, August, October, and December, at**
248 **depths of 0, 20, 50, and 100 m. Specific measurement dates and times were not fixed, so we viewed the measurement data as**
249 **values that represented each month and used them to verify the model.** Data from a model that operated MOM5, the Sea-Ice

250 Simulator, and TOPAZ together (MOM) were used for comparative analysis. MOM was operated using CORE-II forcing
251 data (Large and Yeager, 2009) from 1950 to 2008. We also used data from the Surface Ocean CO₂ Atlas (SOCAT) (Bakker
252 et al., 2016) from the analysis period to verify the CO₂ air-sea gas flux in TOPAZ. The time periods for which SOCAT
253 observational data exists for point 102 are April 2001, January 2005, November 2008, and December 2008. For points 104
254 and 107, the time period is April 2001. Finally, we performed a spin-up for 14 years on the initial data at each point and
255 analyzed the results of operating GOTM-TOPAZ from 1999 to 2008.

256

257 **6 Results**

258 Figure 3 shows the results of the GOTM-TOPAZ simulation and observational data (EN.4.2.1) as vertical distributions of the
259 water column over time. The vertical distributions of salinity are well simulated and are comparable to the observations,
260 although this could also be because relaxation was applied. The water temperature simulated by GOTM-TOPAZ showed a
261 cold bias in the upper layer at a depth of around 120 m. This appears to be the effect of large-scale forcing (from the EKWC)
262 that GOTM-TOPAZ could not resolve. Similar differences in water temperature also appeared at points 104 and 102
263 (Supplementary Figure 1). Observational results showed that the water temperature was particularly affected by the ESIW, a
264 finding that did not appear in the GOTM-TOPAZ results. It was determined that since GOTM-TOPAZ could not reproduce
265 advection from the ESIW, there were differences in the vertical water temperature distributions near depths of 200 m
266 compared to the observational results.

267 We used SeaWiFS data to measure chlorophyll concentrations using light reflected from the ocean surface and thus
268 verified the results simulated by GOTM-TOPAZ. However, part of the reflected light reaches the satellite from the mixed
269 layer below the ocean surface due to a backscattering effect (Jochum et al., 2009; Park et al., 2013). Therefore, we compared
270 chlorophyll anomalies averaged up to 20 m in the data from each model and chlorophyll from SeaWiFS. The mean
271 chlorophyll concentration at depths of 0–20 m, as simulated by GOTM-TOPAZ and MOM, had similar inter-annual
272 variabilities; their correlation coefficients versus the observational data were 0.53 and 0.60, respectively (Fig. 4a), which is
273 statistically significant ($p < 0.001$). In terms of the maximum concentration of chlorophyll that occurred annually on the
274 surface layer, GOTM-TOPAZ showed smaller errors against the observational results than MOM did.

275 Phytoplankton in the East/Japan Sea are generally present in the highest concentrations at depths of around 10–60 m (Rho
276 et al., 2012). Therefore, we averaged chlorophyll concentrations from 20–80 m to verify the model results (Fig. 4b).
277 However, since observational data for chlorophyll in the subsurface layer (~20–80 m) were unavailable, the MOM and
278 GOTM-TOPAZ results were compared instead. There were slight differences in the scale of the minimum and maximum
279 concentrations of chlorophyll in the subsurface layer, but the two models had a correlation coefficient of 0.59 ($p < 0.01$) and
280 a similar inter-annual variability (Fig. 4b). At points 104 and 102, the GOTM-TOPAZ chlorophyll results had a slightly
281 lower correlation coefficient against the observational data than MOM did, but its seasonal variability was similar to the

282 observation data and the results from MOM (Supplementary Figures 2, 5). However, when compared to the results from
283 MOM, the time series of the chlorophyll anomaly in the ocean surface and subsurface layers simulated by GOTM-TOPAZ
284 appear to show a time shift (Fig. 4a, b). In the TOPAZ module in MOM, the transport tendencies of each tracer were
285 calculated in the ocean model; however, this process was not carried out in GOTM-TOPAZ. In addition, MOM and GOTM-
286 TOPAZ are not only just different models of the marine physical environment; the atmospheric forcing data they each use
287 are also different. Therefore, there are complex reasons for the differences in the results of the two models, and further
288 detailed experiments and analysis are required.

289 We evaluated the performance of GOTM-TOPAZ in terms of simulations of dissolved oxygen, nitrogen, phosphorus, and
290 silicon. The sea surface dissolved oxygen levels simulated by GOTM-TOPAZ and MOM had correlation coefficients of 0.47
291 ($p < 0.001$) and 0.50 ($p < 0.001$), respectively, versus the observed data (Fig. 5a). The GOTM-TOPAZ correlation coefficient
292 versus the observed data was 0.31 ($p < 0.001$) for nitrogen, 0.16 ($p < 0.10$) for phosphorus, and 0.19 ($p < 0.05$) for silicon;
293 these were lower than the correlation coefficients between MOM and the observed data (0.36, 0.24, and 0.33, respectively; p
294 < 0.001). However, GOTM-TOPAZ seemed to depict the inter-annual variability of nutrients at the sea surface well (Fig.
295 5b–d). At points 104 and 102, GOTM-TOPAZ showed values for sea surface dissolved oxygen and nutrients with inter-
296 annual variabilities that were similar to the observed data and that from MOM (Supplementary Figures 3, 6).

297 Figure 6 shows a comparison of the vertical profiles of dissolved oxygen, nitrogen, phosphorus, and silicon averaged for
298 February, August, and the entire period from 1999 to 2008. Mixing in the upper ocean occurs actively during winter due to
299 strong winds, and GOTM-TOPAZ well simulated dissolved oxygen (surface to 250 m) and nitrogen (surface to 100 m)
300 concentrations during that season (Fig. 6a). However, for phosphorus and silicon at the same depths, there was a difference
301 between the GOTM-TOPAZ results and the observational data. The concentrations of nitrogen, phosphorus, and silicon
302 simulated by GOTM-TOPAZ from the surface to 60 m decreased during August, and these concentrations were clearly
303 distinguishable from the surface to 60 m due to strong stratification in the summer (Fig. 6b). These stratifications appeared in
304 the observational data. During this season, the oxygen concentration simulated by GOTM-TOPAZ, unlike that in the
305 observational data, increased sharply from depths of 20–60 m. This seems to have been caused by the creation of oxygen
306 from photosynthesis by phytoplankton (Fig. 6b). However, a highly concentrated dissolved oxygen concentration is not
307 apparent in the observational data, because the low dissolved oxygen is transported by the EKWC (Rho et al., 2012). The
308 concentrations of dissolved oxygen from 80–250 m were similar in both the results from GOTM-TOPAZ and in the 10-year
309 observational data (Fig. 6c). However, the differences increased beyond depths of 250 m. We determined that the reason for
310 such differences was due to the inability of GOTM-TOPAZ to reproduce conditions of the ESIW. Nonetheless, the results
311 demonstrated that dissolved oxygen at 80–250 m, nitrogen, and phosphorus are well simulated over 10 years using GOTM-
312 TOPAZ (Fig. 6c). The vertical distributions of dissolved oxygen and nutrients at points 104 and 102 as simulated by GOTM-
313 TOPAZ over the same time period also showed similar patterns as at point 107 (Supplementary Figure 4, 7).

314 Finally, to verify the air-sea gas exchange simulated by GOTM-TOPAZ, we compared the monthly average sea surface
315 CO₂ concentrations in the model and in SOCAT. The correlation coefficient between the sea surface CO₂ concentration
316 simulated by GOTM-TOPAZ and the observational data was 0.94. However, in Fig. 7, there were no more than six months
317 for which the observational values existed at all points; therefore, this is a statistically insignificant value.
318

319 **7 Discussion**

320 In this paper, we explain the major models that comprise GOTM-TOPAZ and the biological-physical feedback loop that they
321 reproduce. In addition, we compiled data from three points of with scientific importance in the East/Japan Sea, near the
322 Korean Peninsula, and analyzed the results of operating GOTM-TOPAZ for a decade (~1999–2008). We compared ocean
323 water temperatures, salinity, and biogeochemical variables such as chlorophyll, dissolved oxygen, nitrogen, phosphorus, and
324 silicon concentrations against the observational data and output from the OGCM to evaluate the performance of GOTM-
325 TOPAZ. The results showed that GOTM-TOPAZ had lower correlation coefficients than OGCM but that it simulated inter-
326 annual variability in a similar manner overall.

327 The SCM (1D model) includes important physical processes and has a much lower computation cost than 3D models; this
328 means that a variety of experiments can be performed repeatedly. With this advantage, 1D models can be useful to track
329 mechanisms that are difficult to understand using 3D models. We believe that TOPAZ, in particular, can be used to obtain
330 insights on the interactions between the chemical makeup and organisms in the ocean because it accounts for complex
331 biogeochemical mechanisms. In addition, the key processes which are studied via TOPAZ can be implemented later into 3D
332 models.

333 A variety of single-column ocean biogeochemical models have already been developed. However, GOTM-TOPAZ
334 includes complex biogeochemical processes and models over 30 kinds of tracers; the other models, which have only simple
335 structures, do not (Dunne et al., 2012b). Furthermore, GOTM-TOPAZ considers the gas transfer caused by changes in the
336 atmosphere and the physical environment of the ocean, depicting the deposition of dissolved iron, lithogenic aluminosilicate,
337 NH₄, and NO₃ due to aerosols. We believe that the sophistication of TOPAZ provides researchers with the opportunity to
338 perform a variety of experiments.

339 For example, the aerosol concentrations are continuously increasing in the over the East Asia region and are known to
340 affect precipitation and atmospheric circulation. Thus, there is a possibility that aerosols affect oceanic biogeochemical
341 processes as deposition occurs into the ocean, and this cannot be ignored. A variety of numerical experiments are necessary
342 to understand this process, but they are difficult to perform using 3D models due to limitations in computing resources.
343 However, as previously noted, GOTM-TOPAZ is fast; as such, it is useful for understanding the biogeochemical changes
344 that occur in the ocean when the concentration of aerosols or CO₂ in the atmosphere changes. In addition, recent studies have
345 reported that the distribution of fisheries is changing due to changes in phytoplankton size structure, caused by upwelling

346 intensity on the coast of the East/Japan Sea (Shin et al., 2017). Phytoplankton of TOPAZ is divided into two-types depending
347 on their size, so it is expected to be useful in above mentioned research.

348 In addition, GOTM-TOPAZ can be used in studies on feedback mechanisms in the biogeochemical and physical
349 environment of the ocean. Sonntag and Hense (2011) used a simple biogeochemistry model linked to GOTM (GOTM-BIO)
350 to analyze the effects of phytoplankton on the physical environment of the upper ocean. The feedback from cyanobacteria,
351 particularly during surface blooms that cause changes in ocean surface albedo, the solar light absorption rate, and the
352 momentum relayed to the ocean by wind were applied to the model during the experiment. Sonntag and Hense (2011)
353 provided us a better understanding of the needs and direction to focus on with GOTM-TOPAZ, and we plan to apply various
354 climate-ocean biogeochemistry feedback mechanisms to it in future research. We also plan to evolve GOTM-TOPAZ into a
355 single ESM by coupling an atmospheric SCM and a model that reproduces atmospheric chemical mechanisms with GOTM-
356 TOPAZ.

357 We separated TOPAZ from MOM and constructed a model with separate initiation and column physics modules, thus
358 introducing the possibility of more easily coupling it with various other ocean models in the future. We are currently
359 conducting a study on coupling TOPAZ with the Nucleus for European Modelling of the Ocean (NEMO), another OGCM
360 that is already coupled with other biogeochemistry models, such as the MEDUSA (Yool et al., 2013), and the PISCES
361 (Aumont et al., 2015). If NEMO and TOPAZ can be coupled successfully, a comparative analysis of the simulation results
362 from the each biogeochemistry model might provide the driving force for improving the modelling of physical processes
363 associated with ocean-biogeochemistry.

364

365 **Code and data availability:**

366 The GOTM-TOPAZ software is based on GOTM version 4 and MOM version 5, both available for download from their
367 respective distribution sites (<https://gotm.net>, <https://www.gfdl.noaa.gov/>). GOTM-TOPAZ is freely available at
368 <https://doi.org/10.5281/zenodo.1405270>.

369

370 **Author contribution:**

371 H.C.J. and B.K.M. drafted the paper, performed the experiments, and were primarily responsible for developing GOTM-
372 TOPAZ. J.W., H.S.P., J.L., and Y.H.B. contributed to code debugging and writing the paper.

373

374

375 **Competing interests:**

376 The authors declare that they have no conflicts of interest.

377

378 **Acknowledgements:**

379 We would like to thank the GOTM and MOM communities for their support. In addition, we would like to thank the
380 European Centre for Medium Range Weather Forecasts for providing ERA-Interim data and Hadley Centre at the Met Office
381 for providing the EN4 datasets. In addition, we would like to thank the National Institute of Fisheries Science for providing
382 ocean observation data and the NASA Goddard Space Flight Center for providing SeaWiFS datasets. We also thank D.H.
383 Kim at Kongju National University of Korea for providing some advice during this research. We appreciate J.H. Choi and
384 H.K. Kim at Chonbuk National University of Korea for their helpful discussion and comments. This work was funded by the
385 Korea Meteorological Administration Research and Development Program under Grant KMI (KMI2018-03513).

386

387 **References**

- 388 Aumont, O., Ethe, C., Tagliabue, A., Bopp, L., and Gehlen, M.: PISCES-v2: an ocean biogeochemical model for carbon and
389 ecosystem studies, *Geosci. Model Dev.*, 8, 2465–2513, doi:10.5194/gmd-8-2465-2015, 2015.
- 390 Azhar, M. A., Canfield, D. E., Fennel, K., Thamdrup, B., and Bjerrum, C. J.: A model-based insight into the coupling of
391 nitrogen and sulphur cycles in a coastal upwelling system, *J. Geophys. Res. Biogeosci.*, 119, 264–285,
392 doi:10.1002/2012JG002271, 2014.
- 393 Bakker, D. C. E., Pfeil, B., Landa, C. S., Metzl, N., O'Brien, K. M., Olsen, A., Smith, K., Cosca, C., Harasawa, S., Jones, S.
394 D., Nakaoka, S.-I., Nojiri, Y., Schuster, U., Steinhoff, T., Sweeney, C., Takahashi, T., Tilbrook, B., Wada, C.,
395 Wanninkhof, R., Alin, S. R., Balestrini, C. F., Barbero, L., Bates, N. R., Bianchi, A. A., Bonou, F., Boutin, J., Bozec, Y.,
396 Burger, E. F., Cai, W.-J., Castle, R. D., Chen, L., Chierici, M., Currie, K., Evans, W., Featherstone, C., Feely, R. A.,
397 Fransson, A., Goyet, C., Greenwood, N., Gregor, L., Hankin, S., Hardman-Mountford, N. J., Harlay, J., Hauck, J.,
398 Hoppema, M., Humphreys, M. P., Hunt, C. W., Huss, B., Ibáñez, J. S. P., Johannessen, T., Keeling, R., Kitidis, V.,
399 Körtzinger, A., Kozyr, A., Krasakopoulou, E., Kuwata, A., Landschützer, P., Lauvset, S. K., Lefèvre, N., Lo Monaco, C.,
400 Manke, A., Mathis, J. T., Merlivat, L., Millero, F. J., Monteiro, P. M. S., Munro, D. R., Murata, A., Newberger, T., Omar,
401 A. M., Ono, T., Paterson, K., Pearce, D., Pierrot, D., Robbins, L. L., Saito, S., Salisbury, J., Schlitzer, R., Schneider, B.,
402 Schweitzer, R., Sieger, R., Skjelvan, I., Sullivan, K. F., Sutherland, S. C., Sutton, A. J., Tadokoro, K., Telszewski, M.,
403 Tuma, M., van Heuven, S. M. A. C., Vandemark, D., Ward, B., Watson, A. J., and Xu, S.: A multi-decade record of high-
404 quality fCO₂ data in version 3 of the Surface Ocean CO₂ Atlas (SOCAT), *Earth Syst. Sci. Data*, 8, 383–413,
405 <https://doi.org/10.5194/essd-8-383-2016>, 2016.
- 406 Betts, A. K., and Miller, M. J.: A new convective adjustment scheme. Part II: Single column tests using GATE wave,
407 BOMEX, ATEX and arctic air-mass data sets, *Q. J. Roy. Meteor. Soc.*, 112, 693–709, doi:10.1002/qj.49711247308,
408 1986.
- 409 Bruggenman, J., and Bolding, K.: A general framework for aquatic biogeochemical models, *Environ. Modell. Softw.*, 61,
410 249–265, doi:10.1016/j.envsoft.2014.04.002, 2014.
- 411 Burchard, H., Bolding, K., Kuhn, W., Meister, A., Neumann, T., and Umlauf, L.: Description of a flexible and extendable
412 physical-biogeochemical model system for the water column, *J. Marine Syst.*, 61, 180–211,
413 doi:10.1016/j.jmarsys.2005.04.011, 2006.
- 414 Cloern, J. E., Grenz, C., and Videgar-Lucas, L.: An empirical model of the phytoplankton chlorophyll: carbon ratio-the
415 conversion factor between productivity and growth rate, *Limnol. Oceanogr.*, 40(7), 1313–1321,
416 doi:10.4319/lo.1995.40.7.1313, 1995.
- 417 De Baar, H. J. W.: von Liebig's law of the minimum and plankton ecology (1899-1991), *Progress. Oceanogr.*, 33, 347–386,
418 1994.

419 Dee, D. P., Uppala, S. M., Simmons, A. J., Berrisford, P., Poli, P., Kobayashi, S., Andrae, U., Balmaseda, M. A., Balsamo,
420 G., Bauer, P., Bechtold, P., Beljaars, A. C. M., van de Berg, L., Bidlot, J., Bormann, N., Delsol, C., Dragani, R., Fuentes,
421 M., Geer, A. J., Haimberger, L., Healy, S. B., Hersbach, H., Hólm, E. V., Isaksen, L., Kållberg, P., Köhler, M.,
422 Matricardi, M., McNally, A. P., Monge-Sanz, B. M., Morcrette, J.-J., Park, B.-K., Peubey, C., de Rosnay, P., Tavolato,
423 C., Thépaut, J.-N., and Vitart, F.: The ERA-Interim reanalysis: configuration and performance of the data assimilation
424 system, *Q. J. Royal Meteorol. Soc.*, 137, 553–597, doi:10.1002/qj.828, 2011.

425 Dirmeyer, P. A., Cash, B. A., Kinter III, J. L., Stan, C., Jung, T., Marx, L., Towers, P., Wedi, N., Adams, J. M., Altshuler, E.
426 L., Huang, B., Jin, E. K., and Manganello, J.: Evidence for enhanced land-atmosphere feedback in a warming climate, *J.*
427 *Hydrometeorol.*, 13, 981–995, doi:10.1175/JHM-D-11-0104.1, 2012.

428 Dunne, J. P., John, J. G., Adcroft, A. J., Griffies, S. M., Hallberg, R. W., Shevliakova, E. N., Stouffer, R. J., Cooke, W.,
429 Dunne, K. A., Harrison, M. J., Krasting, J. P., Malyshev, S. L., Milly, P. C. D., Phillips, P. J., Sentman, L. A., Samuels,
430 B. L., Spelman, M. J., Winton, M., Wittenberg, A. T., and Zadeh, N.: GFDL’s ESM2 global coupled climate-carbon
431 Earth System Models Part I: Physical formulation and baseline simulation characteristics, *J. Clim.*, doi:10.1175/JCLI-D-
432 11-00560.1, 2012a.

433 Dunne, J. P., John, J. G., Shevliakova, E., Stouffer, R. J., Krasting, J. P., Malyshev, S. L., Milly, P. C. D., Sentman, L. T.,
434 Adcroft, A. J., Cooke, W., Dunne, K. A., Griffies, S. M., Hallberg, R. W., Harrison, M. J., Levy, H., Wittenberg, A. T.,
435 Phillips, P. J., and Zadeh, N.: GFDL’s ESM2 global coupled climate–carbon earth system models. Part II: carbon system
436 formulation and baseline simulation characteristics, *J. Clim.*, 26, 2247–2267, doi:10.1175/jcli-d-12-00150.1, 2012b.

437 Evans, T., and Garçon, V.: One-Dimensional Models of Water Column Biogeochemistry; Report of a Workshop held in
438 Toulouse, France; November-December 1995, 1997.

439 Friedlingstein, P., Cox, P., Betts, R., Bopp, L., von Bloh, W., Brovkin, V., Cadule, P., Doney, S., Eby, M., Fung, I., Bala, G.,
440 John, J., Jones, C., Joos, F., Kato, T., Kawamiya, M., Knorr, W., Lindsay, K., Matthews, H. D., Raddatz, T., Rayner, P.,
441 Reick, C., Roeckner, E., Schnitzler, K. G., Schnur, R., Strassmann, K., Weaver, A. J., Yoshikawa, C., and Zeng, N.:
442 Climate-Carbon Cycle Feedback Analysis: Results from the C4MIP Model Intercomparison, *J. Clim.*, 19(14), 3337–3353,
443 doi:10.1175/JCLI3800.1, 2006.

444 Good, S. A., Martin, M. J., and Rayner, N. A.: EN4: Quality controlled ocean temperature and salinity profiles and monthly
445 objective analyses with uncertainty estimates, *J. Geophys. Res. Oceans*, 118, 6704–6716, doi:10.1002/2013JC009067,
446 2013.

447 Gouretski, V., and Reseghetti, F.: On depth and temperature biases in bathythermograph data: development of a new
448 correction scheme based on analysis of a global ocean database, *Deep-Sea Res. Pt. I*, 57, 6, doi:10.1016/j.dsr.2010.03.011,
449 2010.

450 Hartung, K., Svensson, G., Struthers, H., Deppenmeier, A., and Hazeleger, W.: An EC-Earth coupled atmosphere-ocean
451 single-column model (AOSCM) for studying coupled marine and polar process, *Geosci. Model Dev. Discuss.*,
452 doi:10.5194/gmd-2018–66, 2018.

453 Hense, I., Stemmler, I., and Sonntag, S.: Ideas and perspectives: climate-relevant marine biologically driven mechanisms in
454 Earth system models, *Biogeosciences*, 14, 403–413, doi:10.5194/bg-14-403-2017, 2017.

455 Ichiye, T.: Some problem of circulation and hydrography of the Japan Sea and Tsushima Current. In: *Ocean Hydrography of*
456 *the Japan Sea and China Seas*, edited by: Ichiye, T., Elsevier Science Publishers, Amsterdam, 15–54, 1984.

457 Jochum, M., Yeager, S., Lindsay, K., Moore K., and Murtugudde, R.: Quantification of the Feedback between
458 Phytoplankton and ENSO in the Community Climate System Model, *J. Clim.*, 23, 2916–2925,
459 doi:10.1175/2010JCLI3254.1, 2009.

460 Jones, C., and Sellar, A.: Development of the 1st version of the UK Earth system model, UKESM newsletter no. 1 – August
461 2015, available at: <https://ukesm.ac.uk/ukesm-newsletter-no-1-august-2015/> (last accessed: 4 November 2018), 2015.

462 Joo, H. T., Park, J. W., Son, S. H., Noh, J.-H., Jeong, J.-Y., Kwak, J. H., Saux-Picart, S., Choi, J. H., Kang, C.-K., and Lee,
463 S. H.: Long-term annual primary production in the Ulleung Basin as a biological hot spot in the East/Japan Sea, *J.*
464 *Geophys. Res. Oceans*, 119, 3002–3011, doi:10.1002/2014JC009862, 2014.

465 Kawabe, M. Branching of the Tsushima Current in the Japan Sea. Part II: Numerical experiment, *J. Oceanogr. Soc. Japan*, 38,
466 183–192, doi:10.1007/BF02111101, 1982.

467 Kim, D.-W., Jo, Y.-H., Choi, J.-K., Choi, J.-G., and Bi, H.: Physical processes leading to the development of an anomalously
468 large *Cochlodinium polykrikoides* bloom in the East sea/Japan sea, *Harmful Algae*, 55, 250–258,
469 doi:10.1016/j.hal.2016.03.019, 2016.

470 Kim, K., and Chung, J. Y.: On the Salinity-Minimum and Dissolved Oxygen-Maximum Layer in the East Sea (Sea Of
471 Japan), *Elsevier Oceanogr. Ser.*, 39, 55–65, doi:10.1016/S0422-9894(08)70290-3, 1984.

472 Kim, Y.-G., and Kim, K.: Intermediate Waters in the East/Japan Sea, *J. Oceanogr.*, 55, 123–132,
473 doi:10.1023/A:1007877610531, 1999.

474 Krezel, A., Szymanek, L., Kozlowski, L., and Szymelfenig, M.: Influence of coastal upwelling on chlorophyll a
475 concentration in the surface water along the Polish coast of the Baltic Sea, *Oceanologia*, 47(4), 433–452, 2005.

476 Large, W. G. and Yeager, S. G.: The global climatology of an interannually varying air-sea flux data set, *Clim. Dyn.*, 33,
477 341–364, doi:10.1007/s00382-008-0441-3, 2009.

478 Lebassi-Habtezion, B., and Caldwell, P. M.: Aerosol specification in single-column Community Atmosphere Model version
479 5, *Geosci. Model Dev.*, 8, 817–828, doi:10.5194/gmd-8-817-2015, 2015.

480 Lim, H.-G., Park, J.-Y., and Kug, J.-S.: Impact of chlorophyll bias on the tropical Pacific mean climate in an earth system
481 model, *Clim. Dyn.*, doi:10.1007/s00382-017-4036-8, 2017.

482 Lips, I., and Lips, U.: Phytoplankton dynamics effected by the coastal upwelling events in the Gulf of Finland in July-August
483 2006, *J. Plankton Res.*, 32(9), 1269–1282, doi:10.1093/plankt/fbq049, 2010.

484 Litchman, E., Pinto, P. T., Edwards, K. F., Klausmeier, C. A., Kremer, C. T., and Thomas M. K.: Global biogeochemical
485 impacts of phytoplankton: a trait-based perspective, *J. Ecol.*, 103, 1384–1396, doi:10.1111/1365-2745.12438, 2015.

486 Manizza, M., Le Quéré, C., Watson, A. J., and Buitenhuis, E. T.: Bio-optical feedbacks among phytoplankton, upper ocean
487 physics and sea-ice in a global model, *Geophys. Res. Lett.*, 32, L05603, doi:10.1029/2004GL020778, 2005.

488 McClain, C. R., Cleave, M. L., Feldman, G. C., Gregg, W. W., Hooker, S. B., and Kuring, N.: Science quality seawifs data
489 for global biosphere research, *Sea Technol.*, 39, 10–16, 1998.

490 Morel, A., and Antoine, D.: Heating rate within the upper ocean in relation to its Bio-Optical state, *J. Phys. Oceanogr.*, 24,
491 1652–1665, doi:10.1175/1520-0485(1994)024<1652:HRWTUO>2.0.CO;2, 1994.

492 Moriyasu, S.: The Tsushima Current. Kuroshio, Its Physical Aspects, 353–369 pp., 1972.

493 Najjar, R., and Orr, J. C.: Design of OCMIP-2 simulations of chlorofluorocarbons, the solubility pump and common
494 biogeochemistry, Internal report of the Ocean Carbon-Cycle Model Intercomparison Project (OCMIP), 25 pp.,
495 LSCE/CEA Saclay, Gif-sur-Yvette, France, 1998.

496 National Institute of Fisheries Science (NIFS), Korea Oceanographic Data Center, <http://www.nifs.go.kr/kodc>. (accessed
497 May 20, 2018)

498 Park, J.-Y., Dunne, J. P., and Stock, C. A.: Ocean chlorophyll as a precursor of ENSO: An Earth system modeling study,
499 *Geophys. Res. Lett.*, 45, 1939–1947, doi:10.1002/2017GL076077, 2018.

500 Park, J.-Y., Kug, J.-S., Seo, H., and Bader, J.: Impact of bio-physical feedbacks on the tropical climate in coupled and
501 uncoupled GCMs, *Clim. Dyn.*, 43, 1811–1827, doi:10.1007/s00382-013-2009-0, 2013.

502 Price, J. F., Weller, R. A., and Pinkel, R.: Diurnal cycling: Observations and models of the upper ocean response to diurnal
503 heating, cooling, and wind mixing, *J. Geophys. Res. Oceans*, 91, 8411–8427, doi:10.1029/JC091iC07p08411, 1986.

504 **Randerson, J. T., Lindsay, K., Munoz, E., Fu, W., Moore, J. K., Hoffman, F. M., Mahowald, N. M., and Doney, S. C.:**
505 **Multicentury changes in ocean and land contributions to the climate-carbon feedback, *Global Biogeochem. Cycles*, 29,**
506 **744–759, doi:10.1002/2014GB005079, 2015.**

507 Redfield, A. C., Ketchum, B. H., and Richards, F.: The influence of organisms on the composition of sea water, in: *The Sea*,
508 edited by: Hill, M. N., Wiley-Interscience, New York, 2, 26–77, 1963.

509 Rho, T., Lee, T., Kim, G., Chang, K.-I., Na, T., and Kim, K.-R.: Prevailing Subsurface Chlorophyll Maximum (SCM) Layer
510 in the East Sea and Its Relation to the Physico-Chemical Properties of Water Masses, *Ocean and Polar Res.*, 34(4), 413–
511 430, doi:10.4217/OPR.2012.34.4.413, 2012. (in Korean)

512 Sauerland, V., Löptien, U., Leonhard, C., Oschlies, A., and Srivastav, A.: Error assessment of biogeochemical models by
513 lower bound methods (NOMMA-1.0), *Geosci. Model Dev.*, 11, 1181–1198, doi:10.5194/gmd-11-1181-2018, 2018.

514 Shimomura, T. and Miyata K. The oceanographical conditions of the Japan sea and its water systems, laying stress on the
515 summer of 1955, *Bull. Japan Sea Reg. Fish. Res. Lab.*, 6, 23–97, 1957. (in Japanese)

516 Shin, J.-W., Park, J., Choi, J.-G., Jo, Y.-H., Kang, J. J., Joo, H. T., and Lee, S. H.: Variability of phytoplankton size structure
517 in response to changes in coastal upwelling intensity in the southwestern East Sea, *J. Geophys. Res. Oceans*, 122, 10,
518 262–10, 274, doi:10.1002/2017JC013467, 2017.

519 Soden, B. J., and Held, I. M.: An assessment of Climate Feedbacks in Coupled Ocean-Atmosphere Models, *J. Clim.*, 19(14),
520 3354, doi:10.1175/JCLI3799.1, 2006.

521 Sokolov, A., Kicklighter, D., Schlosser, C. A., Wang, C., Monier, E., Brown-Steiner, B., Prinn, R., Forest, C., Gao, X.,
522 Libardoni, A., and Eastham, S.: Description and Evaluation of the MIT Earth System Model (MESH), *J. Adv. Model.*
523 *Earth. Sy.*, 10(8), 1759–1789, doi:10.1029/2018MS001277, 2018.

524 Sonntag, S., and Hense, I.: Phytoplankton behavior affects ocean mixed layer dynamics through biological-physical
525 feedback mechanisms, *Geophys. Res. Lett.*, 38, L15610, doi:10.1029/2011GL048205, 2011.

526 Stock C. A., Dunne, J. P., and John, J. G.: Global-scale carbon and energy flows through the marine planktonic food web: an
527 analysis with a coupled physical–biological model, *Progr. Oceanogr.*, 120, 1–28, doi:10.1016/j.pocean.2013.07.001, 2014.

528 Tanioka, K.: On the Eastern Korea Warm Current (Tosen Warm Current), *Oceanogr. Mag.*, 20, 31–38, 1968.

529 Uda, M.: The results of simultaneous oceanographical investigations in the Japan Sea and its adjacent waters in May and
530 June 1932, *J. Imp. Fisher. Exp. St.*, 5, 57–190, 1934. (in Japanese)

531 Umlauf, L., and Burchard, H.: A generic length-scale equation for geophysical turbulence models, *J. Mar. Res.* 61, 235–265,
532 doi:10.1357/002224003322005087, 2003.

533 Umlauf, L., and Burchard, H.: Second-order turbulence closure models for geophysical boundary layers. A review of recent
534 work, *Cont. Shelf Res.*, 25, 795–827, doi:10.1016/j.csr.2004.08.004, 2005.

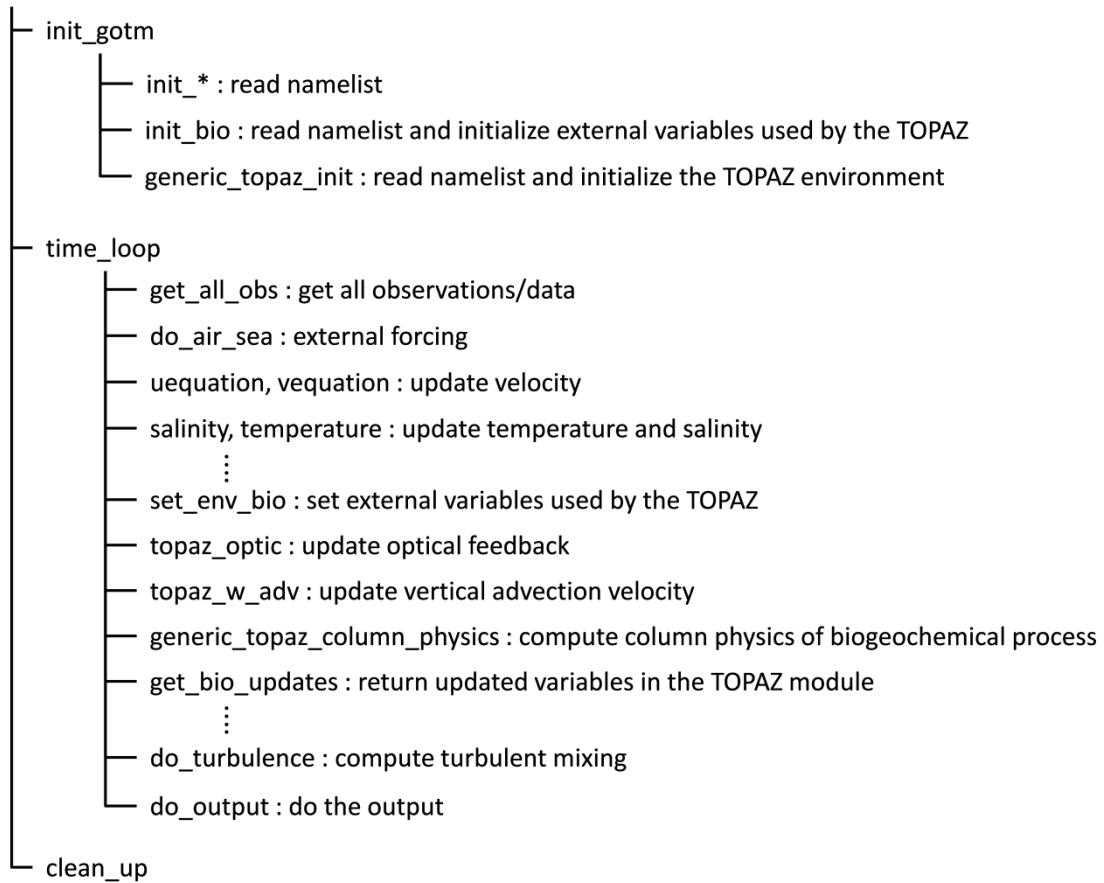
535 Umlauf, L., Burchard, H., and Bolding, K.: General Ocean Turbulence Model. Scientific documentation. v3.2. Marine
536 Science Reports no. 63, Baltic Sea Research Institute Warnemünde, 274 pp., Warnemünde, Germany, 2005.

537 Wanninkhof, R.: Relationship between wind speed and gas exchange over the ocean, *J. Geophys. Res.*, 97, 7373–7382,
538 doi:10.1029/92JC00188, 1992.

539 Yool, A., Popova, E. E., and Anderson, T. R.: MEDUSA-2.0: an intermediate complexity biogeochemical model of the
540 marine carbon cycle for climate change and ocean acidification studies, *Geosci. Model Dev.*, 6, 1767–1811,
541 doi:10.5194/gmd-6-1767-2013, 2013.

542
543
544

GOTM-TOPAZ



546

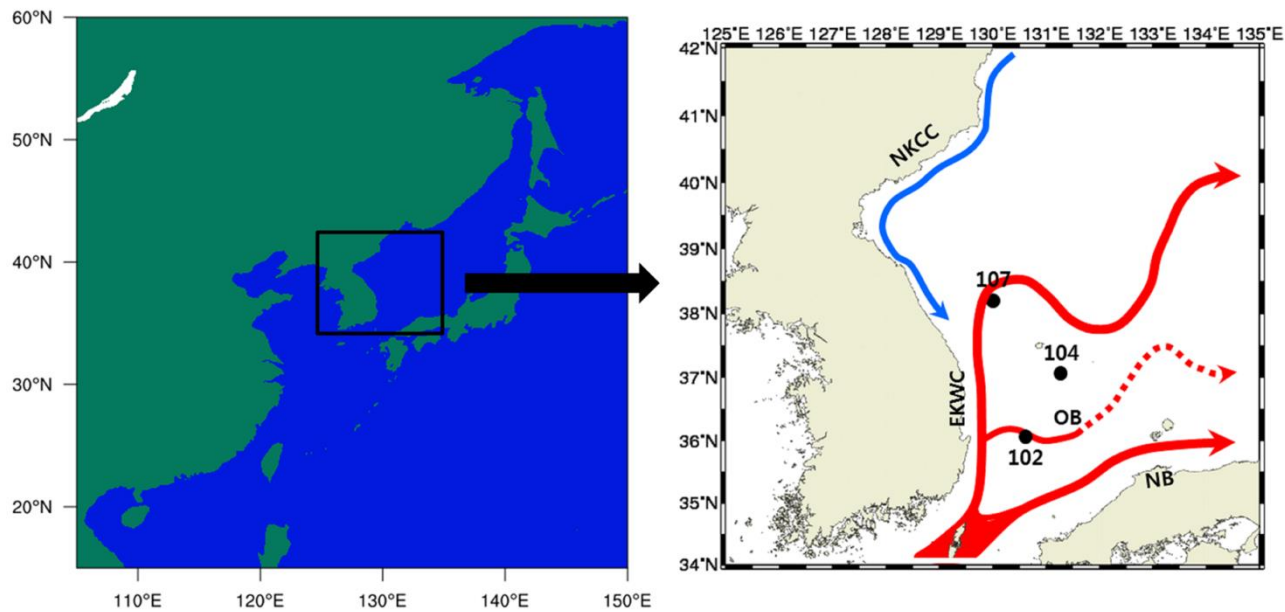
547 **Figure 1: Flow diagram of the Fortran subroutines comprising the Generic Ocean Turbulence Model–Tracers of Phytoplankton**
 548 **with Allometric Zooplankton**

549

550

551

552



553

554

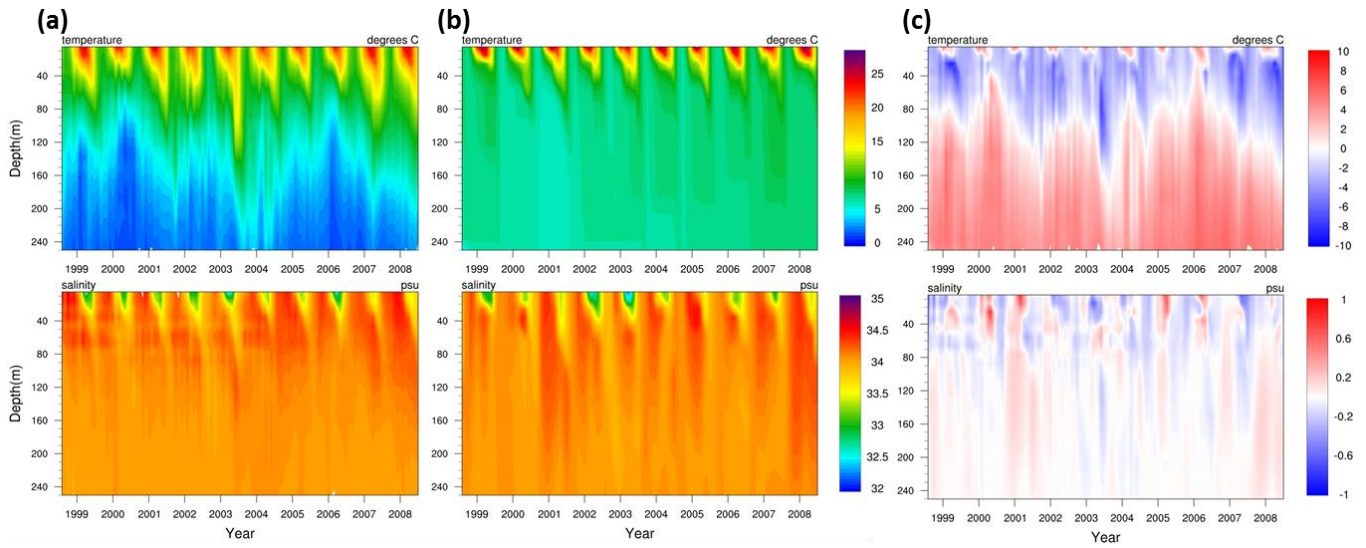
555

556

Figure 2: Location of points (107, 104, 102) in the East/Japan Sea and flow of the nearby North Korea Cold Current (NKCC), East Korea Warm Current (EKWC), Offshore Branch (OB) of the Tsushima Warm Current, and the Nearshore Branch (NB) of the Tsushima Warm Current.

557

558



560

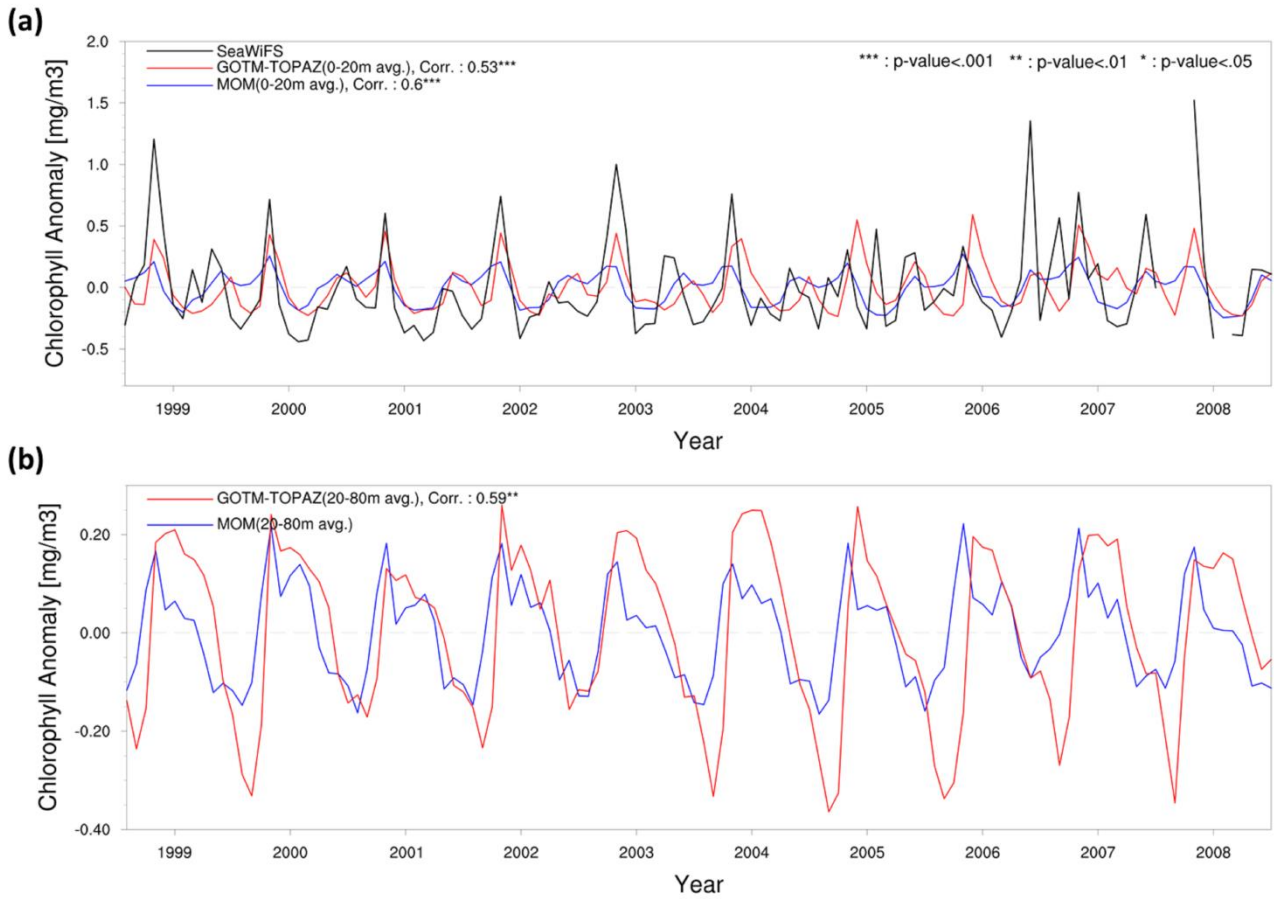
561 **Figure 3: Comparison of the vertical distribution for water temperature [°C], salinity [psu] at point 107 for the 10-year period**
 562 **(1999–2008); (a), (b), and (c) represent observation, GOTM-TOPAZ, and the difference (GOTM-TOPAZ minus observation),**
 563 **respectively.**

564

565

566

567



569

570 **Figure 4: Chlorophyll anomaly time series and correlation values for observational data (black lines), MOM5_SIS_TOPAZ results**
 571 **(blue lines), and GOTM-TOPAZ results (red lines) at point 107 for the 10-year period 1999–2008; (a) the mean value at depths \geq**
 572 **20 m and the correlations between the observations and each model; (b) mean values at depths of 20– 80 m and the correlation**
 573 **between the two models.**

574

575

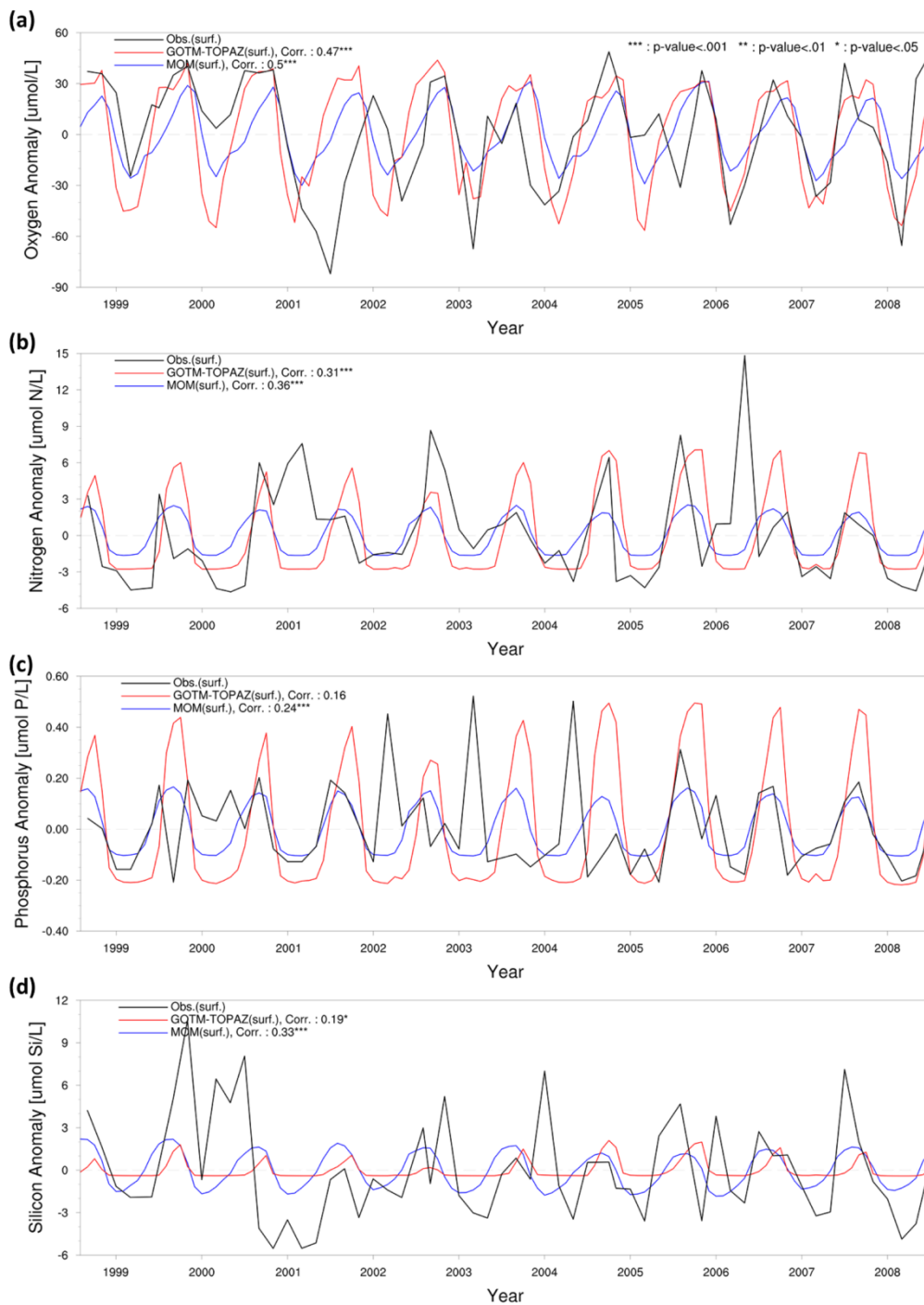
576

577

578

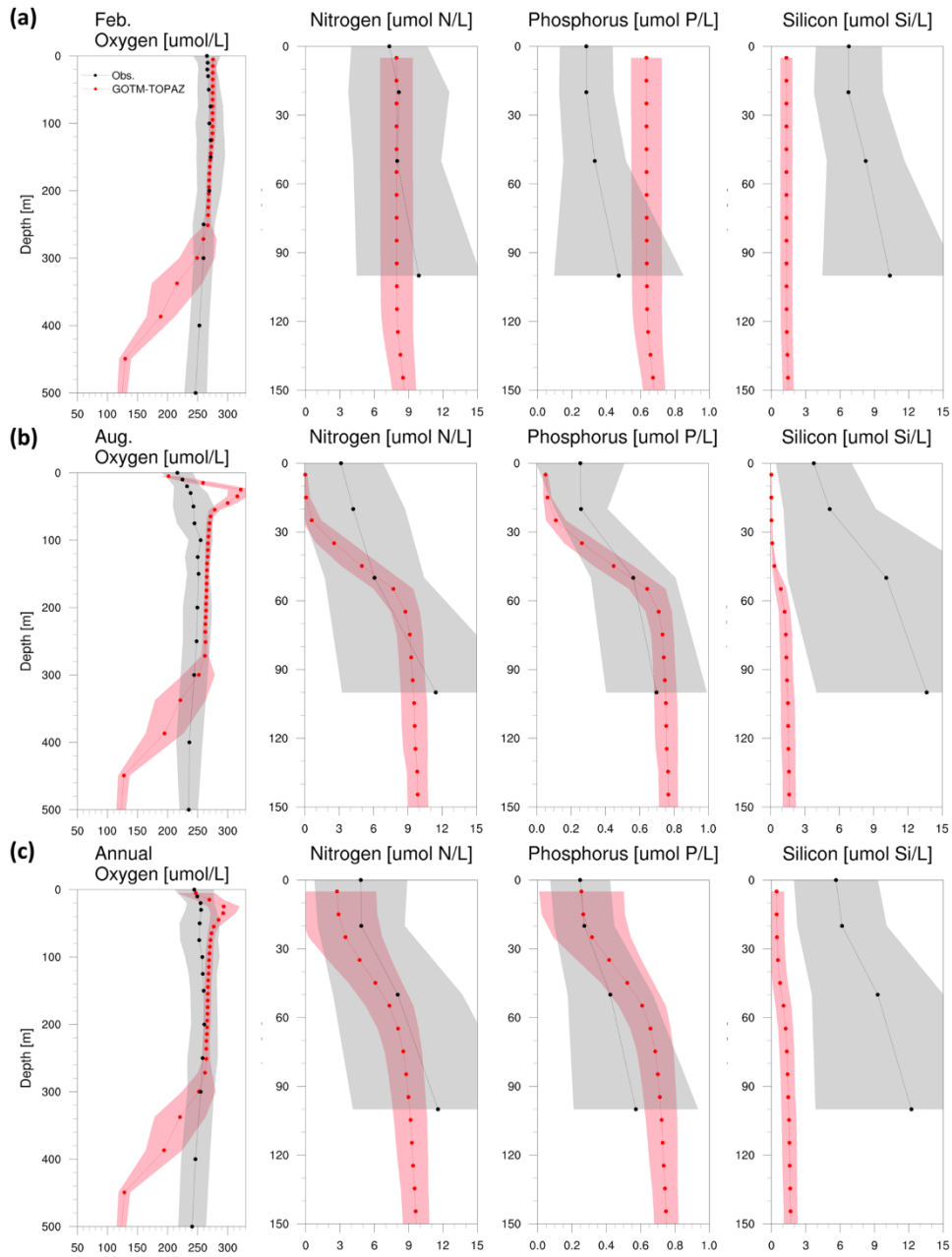
579

580



581

582 **Figure 5: Anomaly time series and correlation values from observational data (black lines), MOM results (blue lines), and GOTM-**
 583 **TOPAZ results (red lines) for concentrations of (a) dissolved oxygen, (b) nitrogen, (c) phosphorus, and (d) silicon at point 107 for**
 584 **the 10-year period 1999–2008; in this figure, nitrogen, phosphorus, and silicon include NO_3 , PO_4 , and SiO_4 , respectively.**



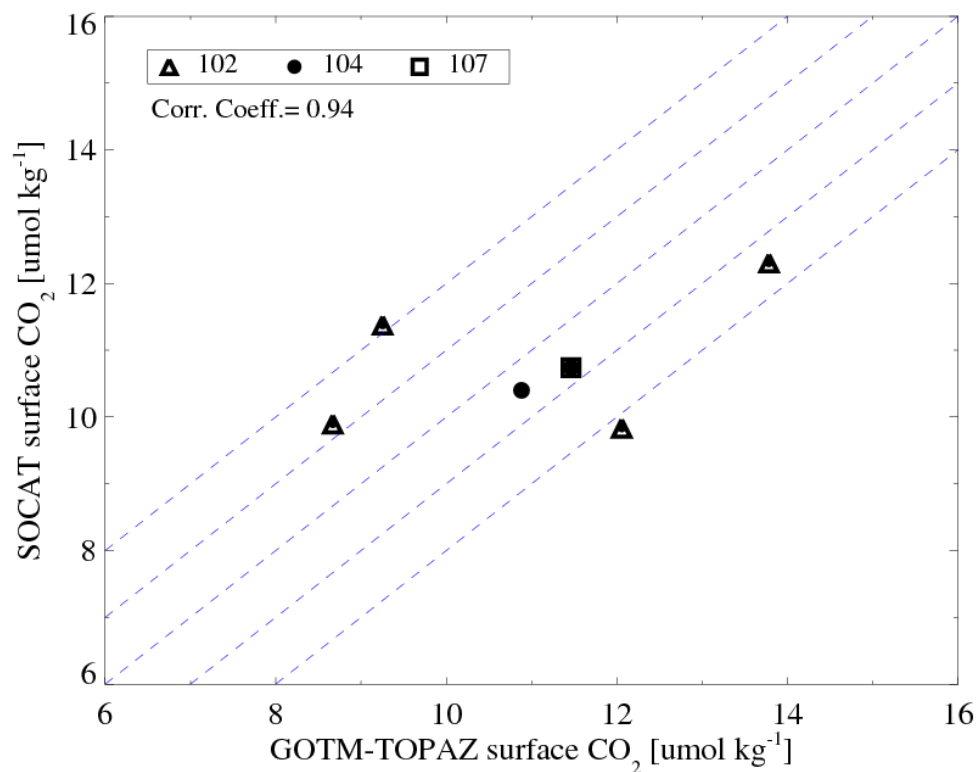
585

586 **Figure 6: Vertical profiles from observational data (black dots) and GOTM-TOPAZ results (red dots) at point 107 for**
 587 **concentrations of dissolved oxygen, nitrogen, phosphorus, and silicon averaged from 1999–2008; (a) for February; (b) for August;**
 588 **and (c) annually. The shaded areas represent 1 sigma. In this figure, nitrogen, phosphorus, and silicon include NO_3 , PO_4 , and SiO_4 ,**
 589 **respectively.**

590

591

592



594

595 **Figure 7: Scatterplot of mean monthly sea surface CO₂ concentration as observed by the Surface Ocean CO₂ Atlas and modelled**
596 **by GOTM-TOPAZ. The thin dotted lines around the 1-to-1 line represents ±1 and 2 μmol kg⁻¹.**

597

Table 1: List of abbreviations

Abbreviation	Full form
ESM	Earth System Model
SCM	Single Column Model
OGCM	Ocean Global Circulation Models
CMIP5	Coupled Model Intercomparison Project 5 (fifth phase)
GFDL	Geophysical Fluid Dynamics Laboratory
ARCCSS	Australian Research Council Centre of Excellence for Climate System Science
NIFS	National Institute of Fisheries Science
ESM2M	Earth System Model version 2, with Modular Ocean Model Version 4.1
ESM2G	Earth System Model version 2, with General Ocean Layer Dynamics
ECMWF	European Centre for Medium-Range Weather Forecasts
GOTM	General Ocean Turbulence Model
TOPAZ	Tracers of Phytoplankton with Allometric Zooplankton
MOM5	Modular Ocean Model version 5
NEMO	Nucleus for European Modelling of the Ocean
MEDUSA	Model of Ecosystem Dynamics, Nutrients Utilization, Sequestration and Acidification
PISCES	Pelagic Interactions Scheme for Carbon and Ecosystem Studies
SOCAT	Surface Ocean CO ₂ Atlas
SeaWiFS	Sea-viewing Wide Field-of-view Sensor
CORE-II	Coordinated Ocean-ice Reference Experiments II
PAR	Photosynthetically Active Radiation
TWC	Tsushima Warm Current
EKWC	East Korea Warm Current
NKCC	North Korea Cold Current
NB	Nearshore Branch
OB	Offshore Branch
ESIW	East Sea Intermediate Water